13B.4 Comparison of Hydrometeor Fall Speed Distributions in Bin and Bulk Microphysical Schemes

Eric A. Aligo*[1,2]
[1] Iowa State University, Ames, Iowa
[2] NOAA/NCEP/EMC-SAIC, Camp Springs, MD

William A. Gallus, Jr.
Iowa State University, Ames, Iowa

Gregory Thompson
National Center for Atmospheric Research, Boulder, CO

Brad S. Ferrier
NOAA/NWS/NCEP/EMC, Camp Springs, MD

1. INTRODUCTION

Since mesoscale convective systems (MCSs) represent the major source of warm-season rainfall for the central and northern Plains (Fritsch et al. 1986), it is important to have high quality rainfall forecasts of such systems. Most numerical modeling studies of MCSs have been based on bulk microphysical schemes. Bulk microphysical schemes assume a size distribution function for each hydrometeor type, and predict one or more moments of that distribution. Schemes that predict one moment of the size distribution often predict the mass content and are referred to as single moment schemes (Rutledge and Hobbs 1983; Lin et al. 1983). Microphysical schemes that predict two moments of the size distribution often predict the number concentration in addition to the mass content (Ferrier 1994; Morrison et al. 2005; Thompson et al. 2008). Some microphysical schemes are triple moment and predict radar reflectivity in addition to number concentration and mass content (Milbrandt and Yau 2005a). Although higher moment bulk schemes have been shown to better represent the sedimentation process, errors in sedimentation still exist (Milbrandt and McTaggart-Cowan 2010).

Bin schemes, unlike bulk schemes, have the advantage of allowing different-sized hydrometeors to exist per model grid point. They predict the mass content and number concentration for an entire spectrum of sizes, and for different hydrometeor categories. Bin schemes are computationally expensive, which is why they are used infrequently in the research community. However, bin schemes should better represent sedimentation compared to bulk schemes.

Lynn and Khain (2007) performed 3D runs of a squall line associated with a sea-breeze event using a spectral (bin) microphysical scheme and several bulk microphysical schemes. The bin scheme had smaller surface convective rain rates and a larger stratiform cloud structure that were both closer to observations. They attributed the improved forecasts to the better representation of sedimentation in the bin scheme, which allowed smaller, slower falling particles to advect away from the updraft.

An objective of this study is to extend the work of Lynn and Khain (2007) by directly comparing the hydrometeor fall speed distributions between bulk and bin schemes, and determining if slower falling hydrometeors exist in the bin scheme. Utilizing idealized simulations of squall lines, these distributions will be examined along with the dominant microphysical processes occurring within regions of slow, moderate, and fast-falling hydrometeors. The model set up and experimental design is described in Section 2, followed by the results in Section 3, a discussion in Section 4 and conclusions in Section 5.

2. DATA AND METHODOLOGY

2.1 Model setup and initial data

Two-dimensional (2D) idealized Weather Research and Forecast (WRF) Advanced Research WRF (ARW) model

* *Corresponding author address*: Eric A. Aligo, NOAA/NCEP/EMC-SAIC, 5200 Auth Road, Camp Springs, MD. Email: eric.aligo@noaa.gov

(Skamarock et al. 2005) simulations were performed using a bin microphysical scheme (Geresdi 1998; Rasmussen et al. 2002; hereafter denoted as Geresdi) in addition to the Lin (Lin et al. 1983), WSM-6 class (Hong and Lim 2006; WSM6) and Thompson (Thompson et al. 2008) bulk microphysical schemes.

Using WRF version 3.0, a series of idealized squall line experiments were performed using three different initial conditions. The primary simulation used a standard input thermodynamic and kinematic input sounding taken from Weisman et al. (1988). A second sounding with greatly reduced upper-atmosphere humidity and increased convective available potential energy (CAPE) was constructed from real data from the 12 June 2002 International H_2O Project (IHOP; Parsons 2002) case. Lastly, a sounding representative of a leading stratiform (LS) system (Parker and Johnson 2004) was used as a third test case. Convection was initiated in the center of the domain by a 4-km radius warm thermal perturbation of magnitude 3 K. A smaller perturbation was used for the 12 June 2002 case to prevent gravity-wave initiated convection from interfering with the main system. The experiments utilized 600 horizontal grid points spaced 1 km apart and 80 vertical levels and simulated 6 hours duration. These simulations used flat terrain, did not consider radiation, surface fluxes or frictional effects, and did not include Coriolis acceleration. The boundary conditions were open in the x-direction and periodic in the y-direction.

2.2 Experimental design

Common between the bin and three bulk schemes, the terminal velocity of each hydrometeor follows a prescribed power law relation from Ferrier (1994):

$$V(D) = \left(\frac{\rho_0}{\rho}\right)^{1/2} \alpha D^{\beta} e^{-fD}, \qquad (1)$$

where ρ_0 is a reference air density usually chosen to be close to the surface, ρ is the air density, D is the diameter of the particle and α, β, and f are constants specified differently in each scheme and for each species (see Table 1). Non-zero f values in the exponential were used only by two hydrometeor species (rain and snow) in the Thompson scheme and all other species in all schemes neglected this term by using a zero value.

Since the bulk schemes need to apply a distribution-weighted value of terminal velocity, they apply the following formula to compute mass-weighted velocity to sediment mixing ratio:

$$\hat{V} \equiv \frac{\int_0^{\infty} V(D)m(D)N(D)dD}{\int_0^{\infty} m(D)N(D)dD}, \qquad (2)$$

where $V(D)$ follows Eq. 1, $m(D) = aD^b$ relates particle mass to diameter, and $N(D)$ is the assumed number distribution of the form:

$$N = N_o D^{\mu} e^{-\lambda D}, \qquad (3)$$

where N_0 is the so-called y-intercept parameter, λ is the distribution slope, and μ is the shape parameter. All of these parameters differ between the various schemes and values of each can be found in the aforementioned references. In addition, the Thompson scheme predicts number concentrations of cloud ice and rain and applies a separate velocity to sediment number of particles using Eq. 2 without the mass relation.

Table 1. Coefficients used in fall velocity relation (Eq. 1) for the indicated hydrometeors of the four microphysical schemes as well as the prescribed reference density, ρ_0.. For graupel fall speeds in Lin, α, varies according to air density. For cloud ice in WSM6, the formula used is: $V = \alpha(\rho \cdot q_i)^{\beta}$, where ρ is the air density with units of kg m^{-3} and q_i is the ice mixing ratio in kg kg^{-1}.

Scheme Hydrometeor	α	β	f	ρ_o
Geresdi				1.20
Water drops	(see Pruppacher and Klett 1997)			
Cloud ice	304	1	0	
Snow	1250	1	(mass < 5.654E-9 kg)	
	4.84	0.25	(mass >= 5.654E-9 kg)	
Graupel	(Rasmussen and Heymsfield 1987)			
Thompson				1.18
Rain	4854	1	195	
Cloud ice	1847.5	1	0	
Snow	40	0.55	125	
Graupel	442	0.89	0	
WSM6				1.28
Rain	841.9	0.8	0	
Cloud ice	1490	1.31	0	
Snow	11.72	0.41	0	
Graupel	330	0.8	0	
Lin				1.29
Rain	841.9	0.8	0	
Cloud ice	3.29	0.16	0	
Snow	4.836	0.25	0	
Graupel	(see caption)	0.5	0	

The Geresdi bin scheme predicts both mass mixing ratio and number concentration of 36 mass-doubling bins for five species.

Therefore, this scheme predicts 360 distinct variables and utilizes a different terminal velocity for each one. In contrast, the bulk schemes predict between five and seven variables and use only one velocity at each model grid point. Clearly, the computational costs of the bin scheme greatly exceed the bulk schemes and restricted this study to idealized 2D experiments.

2.2.1 Microphysical budget

A microphysical budget was computed following Colle et al. (2005):

$$\overline{Pqqqq} = \frac{\sum_{i,k} p^*(i) \times Pqqqq(i,k) \times \Delta\sigma(k)}{\sum_{i,k} p^*(i) \times WVL(i,k) \times \Delta\sigma(k)}, \quad (4)$$

where $Pqqqq(i,k)$ is a microphysical source/sink term averaged for the layer, Δσ, between two model levels, and *p**(i) is the pressure difference between the surface and top of model. The term *WVL(i,k)* is the water vapor loss rate, which differs for each species, but summarizes the loss (or gain) of vapor as a hydrometeor species grows (or diminishes). The budget can be used to identify the most important microphysical processes contributing to the creation of hydrometeors and their associated fall speeds. Colle et al. (2005) performed their budget analysis over a volume fixed in space and time. In this study, however, the budget was evaluated over all times beginning one hour into the simulation, and over portions of the system that contained particles of specified fall speeds. Note that while all of the source/sink terms were accumulated over every model time step (2 seconds), only ten-minute interval output times were used (31 ten-minute intervals altogether) for the budget computations. For a grid point to be considered in the budget, a hydrometeor species had to have a fall speed value within a pre-determined range at the end of the previous 10-min time period and at the end of the current 10-min time period. Clearly *WVL(i,k)* will differ between different schemes but normalizing each source/sink term with water vapor loss should provide insight into the relative importance of certain processes within certain range of fall speeds.

3. Results

The evolution of the idealized squall line is similar among all four schemes and no large differences were noted when changing the initial conditions to the two alternative input soundings. For this reason, the results from the first sounding are used throughout the remainder of the paper. In numerous figures to follow, the following convention is used to simplify interpretation: a blue color represents the slowest falling hydrometeors, red represents the middle range of speeds, and green represents the fastest falling particles. The range of velocities grouped into each category differs for each species.

3.1 Rain

The distributions of fall speed of rain from each microphysics scheme are presented in Fig. 1. The bulk schemes contain two classes of water drops: cloud water, which does not sediment, and rain, which is usually considered to be larger than a threshold diameter. In contrast, the bin scheme contains water drops down to a single micron diameter so a direct comparison of the slowest falling water drops is not warranted. Instead, we will constrain our discussion to fall speeds exceeding approximately 0.1 m s^{-1}. Immediately obvious from Fig. 1 is the broad range of speeds found in the Geresdi bin scheme and more narrow distributions by all of the bulk schemes. The bulk schemes have more similarity to each other than to the bin scheme in the broadest sense, however, there are subtle differences worthy of note. For one, the bin scheme shows evidence of a double-peak around 1.5 m s^{-1} and another around 7 m s^{-1}. Of the bulk schemes, the Thompson and Lin schemes show evidence of a similar double peak. Overall, the Geresdi scheme shows the lowest frequency of the fastest falling rain, which is a topic that will be discussed in more detail below.

To understand better where in the storm a specific range of fall speeds were located, refer to Fig. 2, which shows a vertical cross-section of the storm and three ranges of velocity values within the slow, moderate, and fast-falling categories shown by the blue, red, and green horizontal bars of the previous figure. Regions shown without color either had no rain, like the upper portion of the cloud outline indicated by the grey contour of total condensate, or had terminal velocity values that crossed the thresholds from the start to end of the ten-minute period; for example, where the color changes from red to green. Also contoured in

black are the rain water mixing ratios for each scheme.

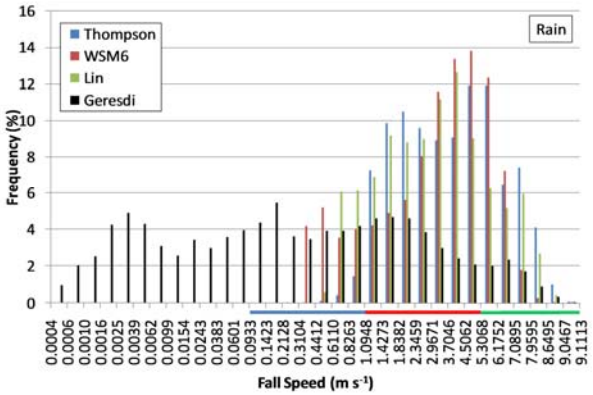

Fig. 1. Rain (in addition to cloud water in Geresdi) fall speed distributions for all schemes as indicated in the inset. Note that rain particles in Geresdi are those with fall speeds above 0.0933 m s^{-1}. The blue, red and green horizontal lines along the abscissa highlight the three fall speed segments used for the vertical cross sections and in the budget analysis in Fig 2. and Fig. 3, respectively

The Geresdi bin scheme (Fig. 2a) shows more parts of the storm with slowly falling rain compared to any bulk scheme, especially towards the rear (left side) centered at about 700 hPa. The Geresdi results also show a very obvious size sorting effect that appears to be mimicked best only by the Thompson scheme (Fig. 2b). The WSM6 results (Fig. 2c) hint at size sorting, however, rain falls fastest between one and three kilometers, then slow down before reaching the surface. The Lin scheme (Fig. 2d) shows hardly any rain above the melting level and no evidence of size sorting.

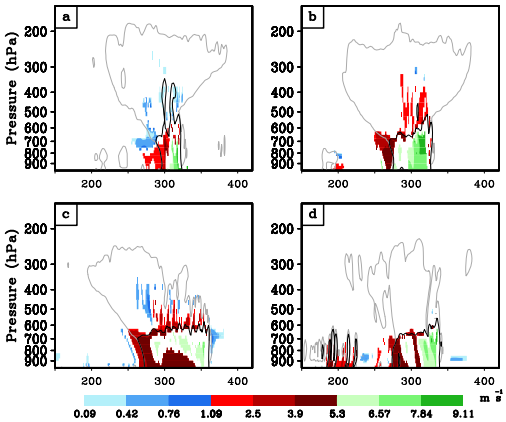

Fig. 2. Vertical cross sections of total condensate (gray contour), rain water mixing ratio (black contour) and rain fall speeds (shaded) four hours into the simulations for (a) Geresdi, (b) Thompson, (c) WSM6 and (d) Lin. In each cross-section, the system is moving from left to right, and the horizontal grid points are located along the abscissa. The 0.01 g kg^{-1} contour is plotted for the total condensate and rain water mixing ratios.

When analyzing the source/sink terms for rain, it was somewhat surprising to see the relative contributions by the various terms differ so much between the various schemes. Fig. 3 shows the primary contributor to rain came from melted ice species in all but the Thompson scheme, and a few obvious differences between bulk schemes are revealed: the Lin scheme was dominated by graupel, not snow; the WSM6 scheme had a bit less graupel and more snow; and the Thompson scheme had the most snow and least graupel. The Geresdi bin scheme rain arose almost entirely from melted graupel and a deeper review of its cause revealed that the graupel sheds it liquid water instantaneously upon melting, rather than allowing some water to cover the graupel surface.

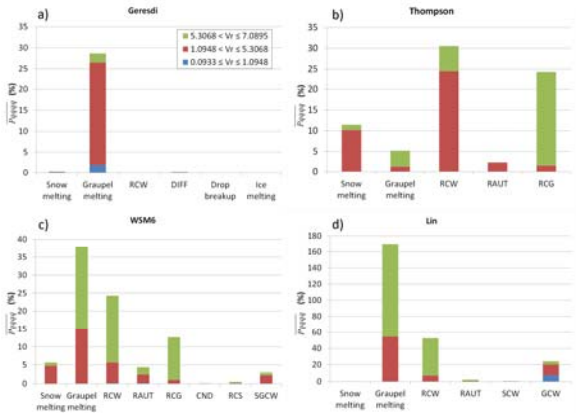

Fig. 3. Percentage contribution of the indicated microphysical processes to the total microphysical budget for particles with different rain fall speeds for (a) Geresdi, (b) Thompson, (c) WSM6 and (d) Lin. Processes indicated for each scheme are those that contribute positively to the rain water mixing ratios. The blue, red and green bars correspond to the fall speed ranges indicated in the inset in (a). Some of the processes are rain collecting cloud water (RCW), water vapor diffuision onto cloud condensation nuclei (DIFF), autoconversion of cloud water to rain water (RAUT), rain collecting graupel (RCG), rain condenstion (CND), snow collecting cloud water (SCW), graupel collecting cloud water (GCW), rain collecting snow (RCS) and accretion of cloud water by averaged snow/graupel (SGCW).

For this reason, a plethora of small droplets are created by the melted graupel, which we believe to be flawed compared to observations. All of the bulk schemes showed a rather significant contribution to rain coming from collection of cloud water, but the relative contributions within certain range of fall speeds differed. Specifically, the Thompson scheme had a larger percentage of rain falling moderately fast and accreting cloud water whereas the other two bulk schemes had faster falling rain that was accreting cloud water. Also, the Thompson

scheme was the only scheme producing rain from collisions between rain and graupel, which would be expected to occur frequently below the melting level in a convective storm

3.2 Snow

The distributions of fall speed of snow for the four schemes are presented in Fig. 4. Compared to the distributions of rain shown in Fig. 1, snow falls very differently between the bulk schemes. Immediately obvious is the large frequency of fast-falling snow in the Lin scheme, with a peak around 1.6 m s^{-1}. This is due to how this scheme implemented constants from a category called "graupel-like snow" from Locatelli and Hobbs (1974). The WSM6 results show a double peak of slowly falling snow about 0.3 m s^{-1} and another peak at 1.3 m s^{-1}. Neither of these two bulk schemes matches the results from the Geresdi bin scheme, however, the Thompson scheme shows very close agreement with a notable match in peak velocity around 0.5 m s^{-1} and a rather broad tail into the larger values as well.

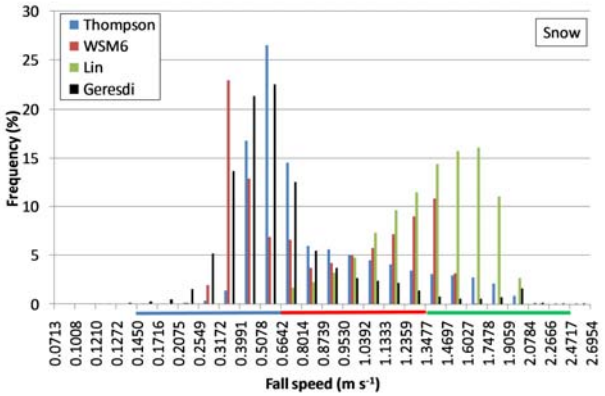

Fig. 4. Snow fall speed distributions for all schemes as indicated in the inset. The blue, red and green horizontal lines along the abscissa highlight the three fall speed segments used for the budget analysis and in the vertical cross sections used in Fig 6. and Fig. 7, respectively.

When the snow fall speeds are plotted in a vertical cross-section, as in Fig. 5, the relatively good comparison between Geresdi and Thompson schemes is confirmed, and both clearly show the effect of size sorting. However, the velocities in Geresdi are generally slower than those found in Thompson. Oddly though, the fastest falling snow in Geresdi is below the melting level and nearly reaches the ground indicating a very likely error in the scheme. The WSM6 snow has a similar pattern to its rain with the fastest-falling snow in the middle of the system, then becoming slower farther down. The Lin scheme is substantially different with fastest falling snow of nearly 2.5 m s^{-1} at the top of the cloud then slower falling snow lower down.

Analysis of the source/sink terms related to snow and categorized by fall speed again revealed some similarities and some differences worth noting. According to Fig. 6, all four schemes showed vapor deposition onto snow as an obvious source of more snow, however results differed to the speed categories in ways similar to each scheme's characteristic fall speeds seen in the previous two figures. All schemes also showed an expected physical result that as snow rimed (SCW), it fell faster. The Geresdi, WSM6, and Lin schemes all showed a contribution to snow by snow collecting cloud ice, whereas the Thompson scheme did not.

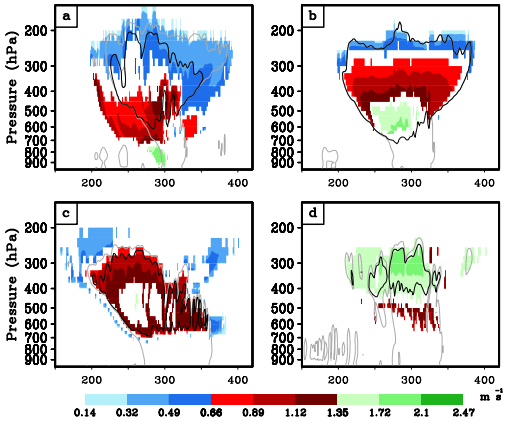

Fig.5. Same as in Fig. 2, but for snow.

3.3 Graupel

Similar to the snow fall speed distributions, the graupel distributions shown in Fig. 7 reveal the highest frequency of fast-falling graupel in the Lin results, a double peak in WSM6 results, and closest match between Geresdi and Thompson results. Also found in the snow distributions, the Geresdi scheme contains more abundant slowly-falling graupel than results from Thompson, but they share nearly the same peak and broad tail of faster-falling particles.

An inspection of the vertical profiles of various categories of fall speed of graupel in Fig. 8 confirms the strong similarities between Geresdi and Thompson results as well as previous results of snow and rain in the WSM6 and Lin experiments. Again, size sorting is not as evident in these latter two schemes.

Additionally, neither the WSM6 nor Lin results show much graupel below the melting level.

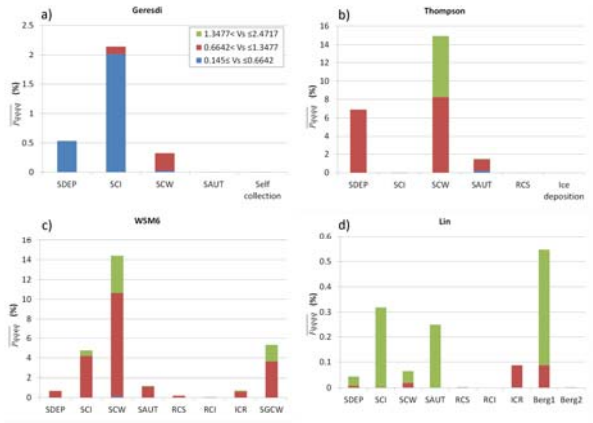

Fig. 6. Same as in Fig. 3 but for snow. Some of the processes are: snow deposition (SDEP), snow collecting ice (SCI), snow collecting water (SCW), autoconversion of cloud ice to snow (SAUT), rain collecting snow (RCS), rain collecting cloud ice (RCI), cloud ice collecting rain (ICR), accretion of cloud water by averaged snow/graupel (SGCW), the reduction of cloud ice by Bergeron process (Berg1), and Bergeron process (deposition and riming)-transfer of cloud water to form snow (Berg2) .

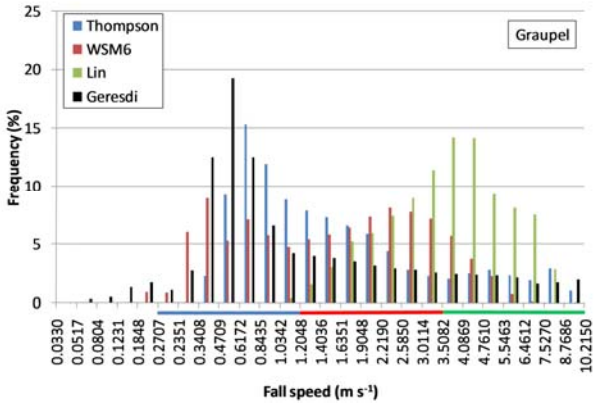

Fig. 7. Graupel fall speed distributions for all schemes as indicated in the inset. The blue, red and green horizontal lines along the abscissa highlight the three segments of fall speeds used in Fig. 8 and Fig. 9.

A review of the various source/sink terms shows dramatically different results between all schemes (Fig. 9). The Geresdi results are dominated by the rain collecting graupel term, which is likely due to the behavior mentioned earlier when melted graupel instantaneously sheds tiny droplets, which then collide again with graupel. The Thompson results show a very broad set of processes responsible for graupel creation including the freezing of large raindrops, rain/snow and rain/ice collisions, graupel accreting cloud water, and rimed snow – all of which makes physical sense. The Thompson results showed almost no contribution to graupel from collisions with rain, probably because the two species fall at similar speeds where they are co-located. In contrast, the WSM6 results showed a dominance of this process, which seems excessive considering that Figs. 2 and 8 show those two species falling at similar speeds where they overlap. The growth of graupel collecting snow and cloud ice were dominant processes in the Lin scheme, consistent with the findings from Lin and Colle (2009), but it is not clear if these are realistic representations of what occurs in actual clouds.

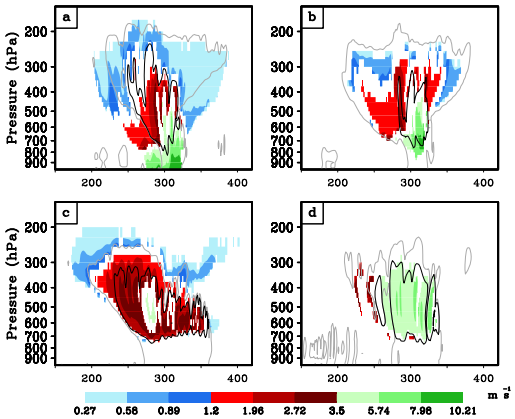

Fig. 8. Same as in Fig. 2, but for graupel.

3.4 Cloud ice

The distributions of fall speeds of cloud ice are shown in Fig. 11. Once again, the Geresdi results showed the highest frequencies of slowly-falling particles and the Thompson results are a reasonable match. Also similar to the previous distributions, the WSM6 and Lin results have more abundant fast-falling cloud ice. In all, the Lin scheme essentially has no ice species falling slowly – they all fall faster than most observations of winter-time snow in eastern Colorado (c.f. Brandes et al, 2007).

The vertical profiles of cloud ice fall speeds reveal the same basic characteristics (Fig. 11) as revealed by the frequency distributions. The results from Geresdi and Thompson are supported by vertically-pointing radar observations of Matrosov et al. 2002. Compared to the other hydrometeors, the source/sink terms are more similar between the schemes with all having vapor deposition onto ice, cloud water droplets freezing and basic nucleation as its sources (Fig. 12).

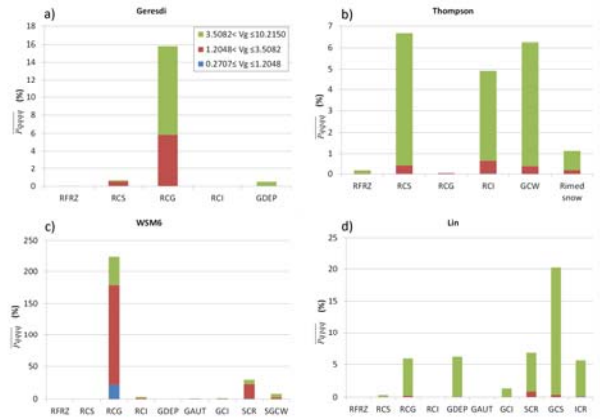

Fig. 10. Same as in Fig. 3 but for graupel. Some of the processes are defined as follows: RFRZ: rain freezing, RCS: rain collecting snow, RCG: rain collecting graupel, RCI: rain collecting ice, GDEP: graupel deposition, RCG: rain collecting graupel, GCW: graupel collecting cloud water, GAUT: autoconversion of snow to graupel, GCI: graupel collecting ice, SCR: snow collecting rain, GCS: graupel collecting snow, ICR: ice collecting rain, SGCW: accretion of cloud water by averaged snow/graupel.

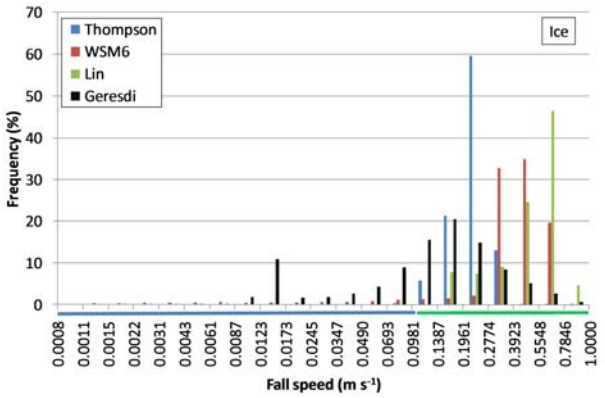

Fig. 10. Cloud ice fall speed distributions for all schemes as indicated in the inset. The blue and green horizontal lines along the abscissa highlight the three segments of fall speeds used in Fig. 11 and Fig. 12.

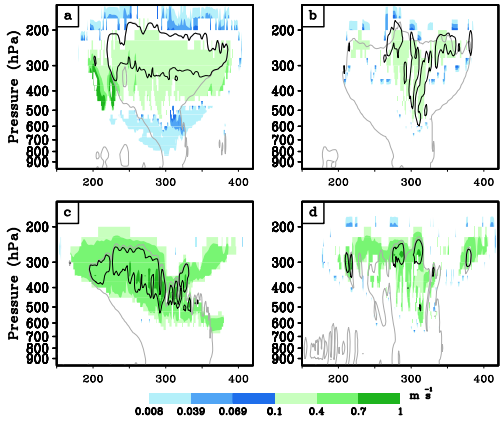

Fig. 11. Same as in Fig. 2, but for cloud ice. The contour level for the ice mixing ratio in the (b) Thompson scheme is 10^{-4} g kg^{-1}, but it is 10^{-2} g kg^{-1} in all other schemes.

4. Discussion

Bin microphysics schemes are often thought to offer a superior advantage over bulk microphysics schemes partly due to their better represention of fall speed distributions (Lynn et al. 2007). From the results using the Thompson scheme, it should be clear that a bulk scheme can capably reproduce the general distribution of fall speeds found using a bin scheme, except, perhaps, the slowest falling particles. The biggest impact of too few slowly-falling particles in simulations of this kind might be a smaller overall stratiform region and anvil produced by the bulk scheme since the hydrometeors sediment quicker rather than carry farther away from the primary convective updraft as they would in the bin scheme. However, the results from the Geresdi bin scheme actually showed a less extensive stratiform and anvil region than the Thompson scheme (compare, for example, Fig. 5a versus 5b).

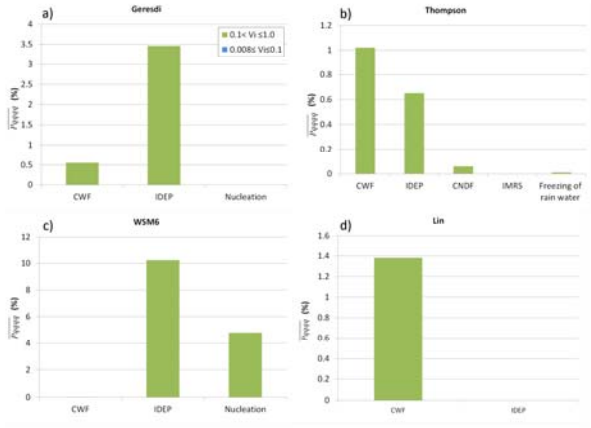

Fig. 12. Same as in Fig. 3, but for cloud ice. Some of the processes are: cloud water freezing (CWF), cloud ice deposition (IDEP), condensation freezing (CNDF), and ice multiplication from rime-splinters (IMRS).

Another representation and comparison of stratiform regions predicted by the various schemes is presented in Fig. 13, which shows a Hovmoller diagram of instantaneous rain rate. The Geresdi scheme predicts a lot of high intensity rain rates spread over a rather broad region, and it also shows the most narrow stratiform region compared to any bulk scheme. The three bulk schemes show varying widths of stratiform regions as well as varying strengths of convective cores. Whereas we might expect the Geresdi scheme to show a broader stratiform region for reasons mentioned earlier, this was not the case. Therefore, we searched for

possible causes and found the Geresdi scheme generally had weaker updrafts, which we attributed to two causes: less latent heat release due to its method of condensing cloud water, and the more numerous small water drops due to the melting ice, which fall to the ground more slowly and delay the creation of a strong cold pool responsible for new convective towers on the leading edge. A time-series plot of the domain-averaged upward vertical velocities predicted using the various schemes is shown in Fig. 14 and reveal generally weaker updrafts in Geresdi than in the three bulk schemes and so less hydrometeors get ejected high into the atmosphere away from the convective core.

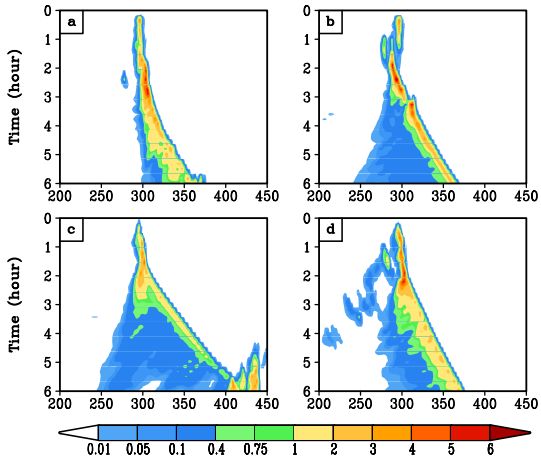

Fig. 13. Hovmoller diagram of rainfall rate (in. h^{-1}; 1 in. = 25.4 mm) for (a) Geresdi, (b) Thompson, (c) WSM6 and (d) Lin. The horizontal grid points are located along the abscissa.

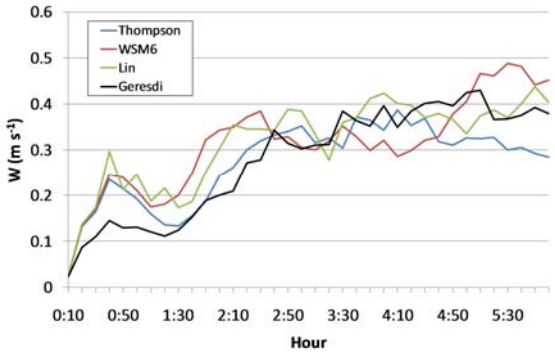

Fig. 14. Time series of domain-averaged upward vertical velocities in m s^{-1} for the microphysical schemes indicated in the inset.

Since the water drops are so numerous and small in the Geresdi scheme, we also expected to see large differences in water evaporation rates, which are presented in Fig. 15. Note that water evaporates approximately three times faster in Geresdi than in the bulk schemes and shows a maximum immediately below the melting level whereas the bulk schemes are more uniform below the melting level all the way to the ground. We believe that if the Geresdi scheme produced fewer small water drops as snow/graupel melted, that it would more likely produce a broader stratiform region than the bulk schemes.

Lastly, whereas some believe that bulk microphysics schemes require two predicted moments to reproduce proper size sorting, this study clearly shows proper size sorting in the Thompson scheme, which has two species, snow and graupel, with one-moment predictive variables and two species that use two-moment predictive variables. The critical parameter responsible for many shortcomings in single-moment microphysical schemes is an imposed constant y-intercept parameter. For decades, single-moment schemes have suffered due to their use of constant intercept parameters, yet observations indicated otherwise. Examples of microphysical schemes that incorporated variable intercept parameters for one or more species include Reisner et al (1998), Thompson et al (2004), Hong et al (2004) and Thompson et al (2008).

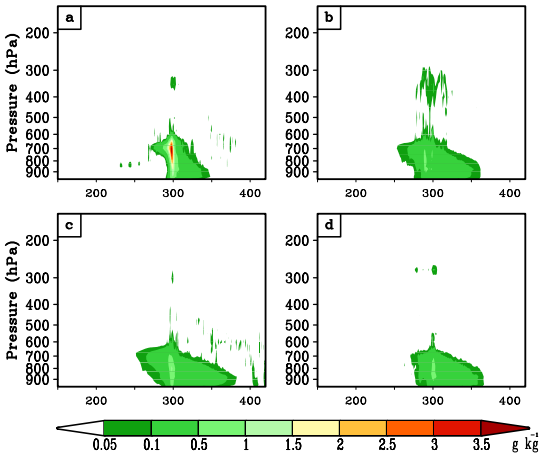

Fig. 15. Vertical cross section of time-domain-averaged liquid (cloud water and rain water) evaporation rate (g kg^{-1} 10 min^{-1}) for (a) Geresdi, (b) Thompson, (c) WSM6 and (d) Lin. The horizontal grid points are located along the abscissa.

5. CONCLUSIONS

Exploratory two dimensional WRF ARW idealized simulations of warm season MCSs were performed to compare fall speed distributions between the Geresdi bin scheme and the Thompson, WSM6 and Lin bulk schemes. In general, results using the Geresdi scheme produced more abundant slowly-falling

hydrometeors than found using any of the bulk schemes. Also, the WSM6 and Lin schemes' fall speed distributions and vertical profiles rarely matched the result of the bin model, whereas the results of the Thompson scheme very closely matched. A number of potential flaws in various microphysical schemes were identified in a budget analysis of the source/sink terms for each hydrometeor:

- The Geresdi scheme instantaneously sheds melt water from melting snow and graupel and likely produces too numerous tiny droplets.
- The Geresdi scheme may not be melting snow properly as it was the only scheme showing snow well below the melting level.
- The WSM6 and Lin schemes show essentially no evidence of proper size sorting.
- The WSM6 and Lin schemes may be melting graupel too aggressively as those results showed hardly any graupel existing below the melting level.
- The Lin scheme clings to the process of graupel collecting snow, which greatly contributes to more graupel, and is not clear if this likely to occur with much frequency in nature since there is no known photographic evidence.

While this study showed that there is the potential for a larger anvil and stratiform region in the Geresdi bin scheme compared with the bulk schemes due to the advection of slower falling particles farther away from the main updraft region, this might have been limited by a weaker system caused by a crude method for dealing with melting ice and a different solution for condensation, which results in less latent heating in the bin scheme. In the near term, the Geresdi scheme will be improved to produce fewer small drops from melted snow and graupel. Also, a study is underway to insert directly the fall speeds found in the bin model to take the place of the fall speeds used within the Thompson scheme.

6. ACKNOWLEDGEMENTS

The authors would like to thank Lulin Xue, Kyoko Ideka, Moti Segal and Chris Karstens for their input. This research was funded by NSF Grants ATM-0848200 and ATM-0537043.

7. REFERENCES

Brandes, E. A., K. Ikeda, G. Zhang, M. Schonhuber, R. M. Rasmussen, 2007: A statistical and physical description of hydrometeor distributions in Colorado snowstorms using a video disdrometer. *J. Climate Appl. Meteor.*, **46**, 634-650.

Colle, B. A., M. F. Garvert, J. B. Wolfe, C. F. Mass and C. P. Woods, 2005: The 13-14 December 2001 IMPROVE-2 event. Part III: Simulated microphysical budgets and sensitivity studies. *J. Atmos. Sci.*, **62,** 3535-3558.

Ferrier, B. S., 1994: A double-moment multiple-phase four-class bulk ice scheme. Part I: Description. *J. Atmos. Sci.*, **51,** 249-280.

Fritsch, J. M., R. J. Kane, and C. R. Chelius, 1986: The contribution of mesoscale convective weather systems to the warm-season precipitation in the United States. *J. Climate Appl. Meteor.*, **25**, 1333-1345.

Geresdi, I, 1998: Idealized simulation of the Colorado hailstorm case: comparison of bulk and detailed microphysics. *Atmospheric Research,* **45**, 237-252.

Hong, S. –H., J. Dudhia and S. –H. Chen, 2004: A revised approach to ice microphysical processes for the bulk parameterization of clouds and precipitation. *Mon. Wea.Rev.,* **132,** 103-120.

_____ and J. O. Lim, 2006: The WRF single-moment 6-class microphysics scheme (WSM6). *Journal of the Korean Meteorological Society,* **42,** 129-151.

Lin, Y, and B. A. Colle, 2009: The 4-5 December 2001 IMPROVE-2 event: Observed microphysics and comparisions with the weather research and forecast model. *Mon.Wea.Rev.,* **137,** 1372-1392.

Lin, Y. –L., R. D. Farley and H. D. Orville, 1983: Bulk parameterization of the snow field in a cloud model. *J. Appl. Meteor.,* **22,** 1065-1092.

Locatelli, J. D. and P. V. Hobbs, 1974: Fall speeds and masses of solid

precipitation particles. *J. Geophys. Res.,* **79,** 2185-2197.

Lynn, B. H., and A. P. Khain, 2007: Utilization of spectral bin microphysics and bulk parameterization schemes to simulate the cloud structure and precipitation in a mesoscale rain event. *J. Geophys. Res.*, **112,** 22205, doi:10.1029/2007JD008475.

Matrosov, S. Y., A. V. Korolev and A. J. Heymsfield, 2002: Profiling cloud ice mass and particle characteristic size from Doppler radar measurements. *J. Atmos. Oceanic Technol.,* **19,** 1003-1018.

Milbrandt, J.A., and M. K. Yau, 2005a: A multimoment bulk microphysics parameterization. Part I: Analysis of the role of the spectral shape parameter. *J. Atmos. Sci.*, **62,** 3051-3064.

_____, and R. McTaggart-Cowan, 2010: Sedimentation-induced errors in bulk microphysics schemes, *J. Atmos. Sci.*, **67,** 3931-3948.

Morrison, H, J. A. Curry, V. I. Khvorostyanov, 2005: A new double-moment microphysics parameterization for application in cloud and climate models. Part I: Description

Parker, M.D. and R. H. Johnson, 2004: Structures and dynamics of quasi-2D mesoscale convective systems, *J. Atmos. Sci.*, **61,** 545-567.

Parsons, D., cited 2002: IHOP_2002 Water Vapor Intercomparisoins Workshop Presentations. [Available online at [http://www.atd.ucar.edu/dir_off/projects/2002/IHOPwsOct03/presentations.html].

Pruppacher, H. R., and J. D. Klett, 1997: *Microphysics of Clouds and Precipitation. Second revised and enlarged edition with an introduction to cloud chemistry and cloud electricity,* Kluwer Academic Publishers, Dordrecht, 954 pp.

Rasmussen, R. M., I. Geresdi, G. Thompson, K, Manning and E. Karplus, 2002: Freezing drizzle formation in stably stratified layer clouds: The role of radiative cooling of cloud droplets, cloud condensation nuclei, and ice initiation. *J. Atmos. Sci.*, **59,** 837-860.

Reisner, J., R. M. Rasmussen, and R. T. Bruintjes, 1998: Explicit forecasting of supercooled liquid water in winter storms using the MM5 mesoscale model. *Quart. J. Roy. Meteor. Soc.*, **124**, 1071-1107.

Rutledge, S. A., and P. V. Hobbs, 1983: The mesoscale and microscale structure and organization of clouds and precipitation in midlatitude cyclones. VIII: A model for the "Seeder-Feeder" process in warm-frontal rainbands. *J. Atmos. Sci.*, **40,** 1185-1206.

Skamarock, W.C., J.B. Klemp, J. Dudhia, D.O. Gill, D.M. Barker, W. Wang, and J.G. Powers, 2005: A description of the advanced research WRF version 2. NCAR Tech. Note NCAR/TN-468+STR, 88 pp. [Available online at http://www.wrf-model.org/wrfadmin/docs/arw_v2.pdf]

Thompson, G, R. M. Rasmussen, K. Manning, 2004: Explicit forecasts of winter precipitation using an improved bulk microphysics scheme. Part I: Description and sensitivity analysis. *Mon.Wea.Rev.,* **132,** 519-542.

_____, P. R. Field, R. M. Rasmussen, and W. D. Hall 2008: Explicit forecasts of winter precipitation using an improved bulk microphysics scheme. Part II: Implementation of a new snow parameterization. *Mon.Wea.Rev.,* **136,** 5095-5115.

Weisman, M. L., J. B. Klemp, and R. Ruttunno, 1988: Structure and evolution of numerically simulated squall lines. *J. Atmos. Sci.*, **45**, 1990-2013.